A frequency independent method for computing the physical optics based electromagnetic fields scattered from a hyperbolic surface

Yu Mao Wu, Weng Cho Chew, Ya-Qiu Jin, Li Jun Jiang, Hongxia Ye, and Wei E. I. Sha

***Abstract*—In this communication, we propose a frequency independent approach, the numerical steepest descent path method, for computing the physical optics scattered electromagnetic field on the quadratic hyperbolic surface. Due to the highly oscillatory nature of the physical optics integral, the proposed method relies on deforming the integration path of the integral into the numerical steepest descent path on the complex plane. Numerical results for the PO based EM fields from the hyperbolic surface illustrate that the proposed numerical steepest descent path method is frequency independent in computational cost and error controllable in accuracy.**

***Index Terms*—Physical optics, hyperbolic surface, numerical steepest descent path, critical point contributions.**

I. Introduction

In electromagnetics (EM), when the product of the external wave number k and the size of the considered object L, i.e., kL ranges from tens to thousands, the analysis of the scattered EM field belongs to the high frequency problem. In this case, the classical physical optics (PO) current approximation [1], has been accepted as an efficient method to calculate the PO based EM fields scattered from the electrically large scatterers. PO based EM fields $\mathbf{E}^{(s)}(\mathbf{r})$ from the considered perfect electric conductor scatterers can be represented as three surface integrals [3] of the type

$$I(k,\mathbf{r}) = \int_{\partial\Omega_1} s(\mathbf{r},\mathbf{r}')e^{ikv(\mathbf{r},\mathbf{r}')}dS(\mathbf{r}'). \tag{1}$$

They are called the surface PO integrals, and $\partial\Omega_1$ denotes the surface of the lit region of the considered object, as shown in Fig. 1. The PO integrand in (1) contains the slowly varying amplitude term $s(\mathbf{r},\mathbf{r}')$, and the exponential of the phase function term $e^{ikv(\mathbf{r}')}$. Due to the highly oscillatory phase behavior of the PO integrand, it is quite challenging to calculate the PO integral with frequency independent workload and error controllable accuracy.

Manuscript received March, 2014; revised November, 2014. This work was supported in part by NSFC 61401103, in part by NSF-SH Grant 14ZR1402400, in part by the talent recruitment under Grant IDH1207001 by Fudan University, in part by State Key Laboratory of Millimeter Waves Grant K201505, in part by Innovation Fund of Petro-China 2014D-5006-0301, in part by SINOPEC Key Lab of Geophysics 33550006-14-FW2099-0034, in part by the Research Grants Council of Hong Kong (GRF 712612 and 711511), in part by US AR120018 contracted through UTAR, and in part by USA NSF CCF Award 1218552.

Yu Mao Wu, Ya-Qiu Jin and Hongxia Ye are with the Key Laboratory for Information Science of Electromagnetic Waves (MoE), Fudan University, Shanghai 200433, China.

Weng Cho Chew is with Department of Electrical and Computer Engineering, University of Illinois at Urbana-Champaign, Urbana, IL 61801 USA (on part-time appointment with HKU), (E-mail: w-chew@uiuc.edu), corresponding author.

Li Jun Jiang and Wei E. I. Sha are with Department of Electrical and Electronic Engineering, The University of Hong Kong, Hong Kong, China.

For the calculation of the PO based EM fields, direct PO solvers [4]- [5] make the computational cost dramatically increase with k. In this sense, efficient algorithms for calculating the PO based EM fields, especially frequency independent algorithms, are in great demand. The traditional high frequency asymptotic (HFA) approach [6]- [10], can provide the calculation of the PO based EM fields with frequency independent workload. In [10], the authors treated the PO integrals from a curved surface with curvilinear edges and relatively general boundary conditions. The canonical integrals in the uniform geometrical theory of diffraction (UTD) were used in the evaluation of PO integrals. Furthermore, the authors developed the efficient algorithm to calculate the "transition functions" in canonical integrals [11]- [12].

Recently, the numerical steepest descent path (NSDP) approach [16]- [20], provides an efficient way to evaluate the highly oscillatory PO integral. The similarity of our work and the work in [17] is that the contour deformation technique via steepest descent paths on the complex plane is adopted to evaluate these PO integrals. However, there are three main differences between these two works. First, in [17], the Abel's summation method, the Lebesgue integral theory and poles extraction technique in complex analysis were adopted for the development of NSDPs from the hyperbolic phase term. In this work, we avoid the Abel's summation and the Lebesgue integral theory and obtain all NSDPS. Second, in [17], the phase function $g(x,y) = xy$ is considered. In this work, the phase function $g(x,y) = x^2 \pm y^2$ is considered via affine transformation technique. Hence, the NSDPs obtained in this paper are different from those in [17]. Importantly, we provide the NSDPs. Third, high frequency wave physics, like the contributions from the stationary phase point, the boundary resonance points and the vertex points, was captured by the proposed NSDP method. In [21], for the computation of scattering from rough surfaces with very large surface heights, an acceleration algorithm was successfully developed by the steepest descent path contour deformation for the Hankel function. In [22], the equivalence between the modified edge representation line and the PO surface integration was developed by the Stokes theorem and the asymptotic technique. Furthermore, a criterion on the acceleration of the PO surface integration with the stationary phase point method was clearly given.

The contributions in this work are that the PO based EM fields from the hyperbolic patches are considered. Then, the integrand of the PO integral takes the hyperbolic phase behavior, which is different from the work in [19]. In this case, all NSDPs are changed and re-constructed compared to the work in [19]. With the high frequency wave physics viewpoint, the formulations of the stationary phase point and the boundary resonance point are all changed. Furthermore, the coalescence of high frequency critical points is considered. We have considered the PO based EM fields from the parabolic and hyperbolic quadratic surfaces, and have further adopted the numerical steepest descent path algorithm knowledge to calculate the scattered fields.

The rest of this paper is organized as follows. In Section II, the PO based EM fields from the hyperbolic surface is

discussed. In Section III, the surface PO integral is first transformed into several highly oscillatory line integrals. Then, we propose the NSDP method to treat these highly oscillatory line integrals. High frequency critical point contributions on the derived NSDPs are extensively studied in Section IV. In Section V, numerical experiments are shown to verify the efficiency of the proposed NSDP method. We make the conclusions in Section VI.

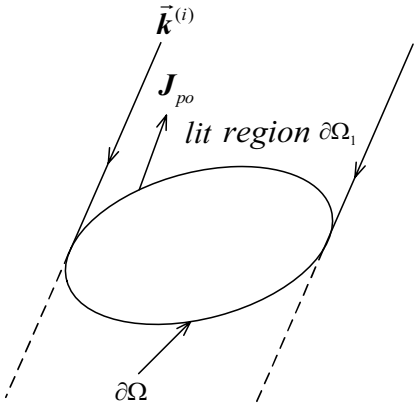

Fig. 1. PO current on the perfect electric conductor scatterer.

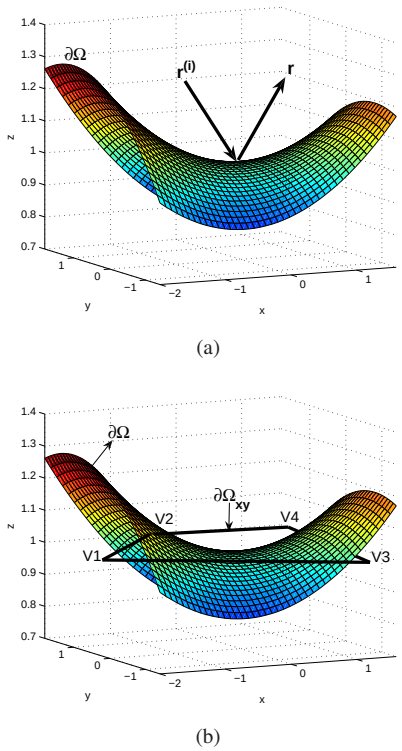

Fig. 2. (a) The electromagnetic wave impinges on the quadratic hyperbolic surface $\partial\Omega$, governed by equation $z = f(x, y)$. (b) The projection of $\partial\Omega$ onto the x-y plane, $\partial\Omega_{xy}$.

II. Surface Physical Optics Integral on the Quadratic Hyperbolic Surface

In this paper, the time harmonic dependence of $e^{-i\omega t}$ is adopted for the EM wave. We consider that the EM wave is impinging on the quadratic hyperbolic surfaces $\partial\Omega$, as demonstrated in Fig. 2(a). The hyperbolic surface is governed by the quadratic equation $z = f(x, y)$, i.e., $f(x, y)$ is a second order polynomial in the xy cartesian coordinate system.For the PEC with the electric conductivity $\sigma = \infty$, we denote the size of the considered hyperbolic surface as $L = \text{diam}(\partial\Omega)$, and the distance of the observation point $\mathbf{r}$ to the origin as $r = |\mathbf{r}|$.

In this work, we consider the far-zone of the scatterer with $r \gg 2L^2/\lambda$ and the PO approximation of the accurate electric equivalent current. λ is the wavelength. Then, for the incident plane wave, $\mathbf{E}^{(i)}(\mathbf{r}) = \mathbf{E}_0{}^{(i)} e^{ik\hat{\mathbf{r}}^{(i)}\cdot\mathbf{r}}$, the PO based EM fields can be written in (1), with

$$\mathbf{s}(\mathbf{r}, \mathbf{r}') = -\frac{ike^{ikr}}{2\pi r}\hat{\mathbf{r}} \times \hat{\mathbf{r}} \times \left(\hat{\mathbf{n}}(\mathbf{r}') \times \hat{\mathbf{r}}^{(i)} \times \mathbf{E}_0{}^{(i)}\right) \quad (2)$$

$$v(\mathbf{r}, \mathbf{r}') = \left(\hat{\mathbf{r}}^{(i)} - \hat{\mathbf{r}}\right) \cdot \mathbf{r}'. \quad (3)$$

In (2)-(3), $\hat{\mathbf{r}} = \mathbf{r}/r$ and $\hat{\mathbf{r}}^{(i)} = \hat{\mathbf{k}}^{(i)}$ are the unit vector of $\mathbf{r}$ and the unit vector of $\mathbf{k}^{(i)}$, respectively. And $\hat{\mathbf{n}}(\mathbf{r})$ is the outward unit normal vector from the hyperbolic surface. Equations (1-3) are the bistatic scattered electric field under the PO approximation. The vector function $\mathbf{s}(\mathbf{r}')$ in (2) is known as the vector amplitude function, and $v(\mathbf{r}')$ in (3) is the phase function. The integrand of the vector PO surface integral in (1) is highly oscillatory when k goes large. The highly oscillatory property of the PO integrand makes the computational effort grow up dramatically with the increasing k, as depicted in Fig. 3(a). Furthermore, for the quadratic surface , the PO integrand of the scattered field in (1), contains the quadratic phase function term $v(x, y)$ [19]. With the asymptotic technique, the steepest descent path method could be adopted to evaluate the PO integral in an efficient way.

To simplify the PO surface integral in (1) to its canonical form, we follow the procedure in [19]. First, we proceed the projection process from the surface $\partial\Omega$ to $\partial\Omega_{xy}$ with polygonal boundary in the $x'y'$ plane, as shown in Fig. 2(b). Next, we conduct the affine transformation as that given in [19], $\partial\Omega_{xy}$ is transformed to another polygonal domain D. In this manner, the PO integral from the hyperbolic surface can be simplified into the following two canonical forms

$$I = \int_D p(x', y') e^{\pm ik\left(-x'^2 + y'^2\right)} dy' dx'. \quad (4)$$

The x' and y' variables in the above integrand correspond to the integration variables in the $x'y'$ plane. The amplitude function $p(x', y')$ takes the formulation

$$p(x', y') = \alpha_1 + \alpha_2 x' + \alpha_3 y' + \alpha_4 x'^2 + \alpha_5 y'^2 + \alpha_6 x' y' \quad (5)$$

and α_j are complex numbers, $j = 1, 2, \cdots, 6$. Here, the domain D is a polygonal domain on the x'-y' plane. In detail, we first decompose the surface into several smaller triangular patches. Hence, the polygonal boundary is formed after the discretization procedure.

III. The Numerical Steepest Descent Path Method

We assume D as the trapezoidal domain in (4), as shown in Fig. 3(b). We denote the x-values of vertex points $\mathbf{V}_1$ and $\mathbf{V}_2$

as L_1 and L_2, respectively. The governing line equation for edge $\mathbf{V}_3\mathbf{V}_4$ is $y = ax + b$, with $a > 0$. The slope "a" of the edge $y = ax+b$ could also be $a < 0$. Then, after a projection of the 3-D surface to a plane of (x, y), the PO surface integral could be simplified into highly oscillatory line integrals in the following way

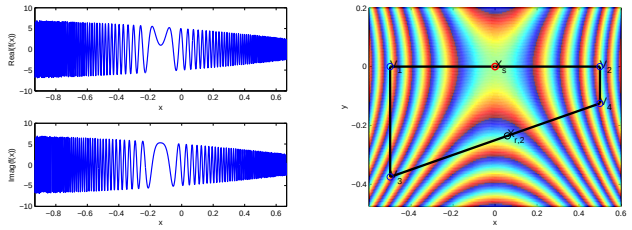

(a) (b)

Fig. 3. (a) Highly oscillatory PO type integrand, $f(x) = (5 - 3x - x^2)e^{ik(-x^2+(ax+b)^2)}$, with $k = 500$. (b) The integration domain is defined on $\mathbf{V}_1\mathbf{V}_2\mathbf{V}_3\mathbf{V}_4$, $[L_1, L_2] \times [ax + b, 0]$ for integrand $e^{ik(-x^2+y^2)}$ with $a = 0.25$, $b = -0.5$.

$$\begin{aligned} I^{(a,b)} &= \int_{L_1}^{L_2}\int_{ax+b}^{0} p(x',y')e^{ik\left(-x'^2+y'^2\right)}dy'dx' \\ &= \int_{L_1}^{L_2}\left(J_2^{(0,0)}(x') - J_2^{(a,b)}(x')\right)e^{-ikx'^2}dx'. \quad (6) \end{aligned}$$

Here, the coordinate system for (x, y) is defined with respect to the use of the polygonal boundary. $J_2^{(0,0)}(x)$ and $J_2^{(a,b)}(x)$ have the formulations

$$J_2^{(0,0)}(x) = j_1(x) + j_2^{(0,0)}(x),$$

$$J_2^{(a,b)}(x) = j_1(x)\,\mathrm{erfc}\left(\sqrt{-ik}(ax+b)\right) + j_2^{(a,b)}(x)\,e^{ik(ax+b)^2}.$$

where

$$j_1(x) = -\frac{\sqrt{\pi}}{2\sqrt{-ik}}\left(\alpha_1 + \alpha_2 x + \alpha_4 x^2 - \frac{\alpha_5}{2ik}\right),$$

$$j_2^{(a,b)}(x) = \frac{\alpha_3 + \alpha_6 x + \alpha_5(ax+b)}{2ik}, j_2^{(0,0)}(x) = \frac{\alpha_3 + \alpha_6 x}{2ik}.$$

Hence, the original PO integral $I^{(a,b)}$ in (6) can be rewritten as

$$I^{(a,b)} = I_2^{(0,0)} - I_2^{(a,b)} \quad (7)$$

where

$$\begin{aligned} I_2^{(a,b)} &= \int_{L_1}^{L_2} J_2^{(a,b)}(x')e^{-ikx'^2}dx' \\ I_2^{(0,0)} &= \int_{L_1}^{L_2} J_2^{(0,0)}(x')e^{-ikx'^2}dx'. \quad (8) \end{aligned}$$

Here, $I_2^{(a,b)}$ and $I_2^{(0,0)}$ are line integrals associated with edges $\mathbf{V}_1\mathbf{V}_2$ and $\mathbf{V}_3\mathbf{V}_4$, respectively. $J_2^{(a,b)}(x)$ has complicated formulations involving the complementary error functions. Importantly, the difference between this paper and the paper in [19] is that the phase term e^{-ikx^2} was adopted in this work, while e^{ikx^2} was considered in [19]. This difference is due to the consideration of the hyperbolic surface in this paper.

The integrand $J_2^{(a,b)}(x)$ in (8) has the following asymptotic behavior

$$J_2^{(a,b)}(x) = \begin{cases} \varsigma_1(x)e^{ik(ax+b)^2}, & x \in \mathcal{D}_1 \\ 2j_1(x) + \varsigma_2(x)e^{ik(ax+b)^2}, & x \in \mathcal{D}_2 \end{cases} \quad (9)$$

with $\varsigma_1(x)$ and $\varsigma_2(x)$ denoted as slowly varying functions.

$\mathcal{D}_1$ and $\mathcal{D}_2$ are the domains separated by the Stokes' line on the complex plane, with the expressions

$$l_{\text{Stokes}}(x) : \mathrm{Im}(x) = -\mathrm{Re}(x) - \frac{b}{a} \quad (10)$$

$$\mathcal{D}_1 := a\left(\mathrm{Re}(x) + \mathrm{Im}(x)\right) + b > 0 \quad (11)$$

$$\mathcal{D}_2 := a\left(\mathrm{Re}(x) + \mathrm{Im}(x)\right) + b < 0. \quad (12)$$

For the case $x \in \mathcal{D}_2$ in (9), the first term $2j_1(x)$ comes from the Stokes' phenomenon of the complementary error function as shown in Fig. 4, details could be found in [19]. After

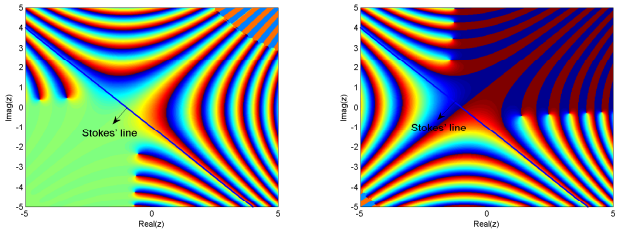

Fig. 4. Stokes' phenomenons of the complementary error functions, $\mathrm{erfc}\left(\sqrt{-ik}(0.5x+1)\right) - 2$ and $\mathrm{erfc}\left(\sqrt{-ik}(0.5x+1)\right)$.

substituting (9) into (8), we get two phase function terms for $I_2^{(a,b)}$. They are

$$g_1(x) = -x^2 + (ax+b)^2, \quad g_2(x) = -x^2. \quad (13)$$

The Stokes' phenomenon of complementary error function makes the phase behaviors of the PO integrand $I_2^{(a,b)}$ be discontinuous.

Now we consider the phase function $g_1(x)$ of $I_2^{(a,b)}$ in (13). Physically, there may exist a point x_s, at which the phase behavior of $g_1(x)$ is different from others. It is called the stationary phase point (SPP). SPP corresponds to the point at which the specular reflection occurs in the high frequency ray physics regime. Mathematically, the SPP x_s satisfies the condition $g_1'(x_s) = 0$. As a result, we have the expression of x_s as

$$x_s = \begin{cases} \frac{ab}{1-a^2}, & |a| \neq 1 \\ \text{no stationary phase point}, & |a| = 1. \end{cases} \quad (14)$$

Remark 1. For the case $|a| = 1$ in the above formulation, the phase function in (13) reduces to a linear form $g_1(x) = 2abx + b^2$. Hence, there is no stationary phase point.

Now we see the term $e^{ikg_1(x)}$ in the PO integrand

$$e^{ikg_1(x)} = e^{ik\left[\mathrm{Re}(g_1(x))+i\mathrm{Im}(g_1(x))\right]} = e^{-k\,\mathrm{Im}(g_1(x))+ik\,\mathrm{Re}(g_1(x))}. \quad (15)$$

Here, $g_1(x)$ is a real function. In this work, we adopt the NSDP method. We consider the real and imaginary parts for the consideration of the NSDP on the complex plane. The NSDP method relies on the transformation of the above highly oscillatory functions to exponential decay functions on the

complex plane. In detail, for a starting point L_*, we define a complex path function $x = \varphi_{L_*}(p)$ as that in [2], satisfying the following identity

$$-\varphi_{L_*}(p)^2 + (a\varphi_{L_*}(p) + b)^2 = -L_*^2 + (aL_* + b)^2 + ip^l \quad (16)$$

with $l = 1$ for integration end points L_1 and L_2, and $l = 2$ for the SPP x_s, respectively. Here, p is the path parameter for the path function on the complex plane. In equation (16), L_* could be used to represent the integration end points L_1 and L_2, as demonstrated in Fig. 4.

After substituting L_1, L_2 and x_s into (16), the corresponding NSDPs are

$$\varphi_{L_m}(p) = \begin{cases} \frac{\mathrm{sgn}(L'_m)}{\sqrt{a^2-1}}\sqrt{{L'_m}^2 + ip} + x_s, & \text{if } |a| > 1 \\ \frac{\mathrm{sgn}(L'_m)}{\sqrt{1-a^2}}\sqrt{{L'_m}^2 - ip} + x_s, & \text{if } |a| < 1 \\ L_m + \frac{ip}{2ab} & \text{if } |a| = 1 \end{cases} \quad (17)$$

$$\varphi_{x_s}(p) = \begin{cases} \frac{\sqrt{ip}}{\sqrt{|1-a^2|}} + x_s, & \text{if } |a| > 1 \\ \frac{\sqrt{-ip}}{\sqrt{|1-a^2|}} + x_s, & \text{if } |a| < 1 \\ \text{no NSDP}, & \text{if } |a| = 1 \end{cases} \quad (18)$$

with $p \in [0, \infty)$ and $p \in (-\infty, \infty)$ in (17) and (18), respectively. Here,

$$L'_m = \sqrt{|1-a^2|}\left(L_m - \frac{ab}{1-a^2}\right) = \sqrt{|1-a^2|}(L_m - x_s),$$

$m = 1, 2$. For instance, the diagrams of NSDPs in (17) and (18) with $|a| = 1$, $|a| > 1$, and $|a| < 1$, are demonstrated in Fig. 5(b)-Fig. 5(d), which correspond to three NSDPs defined on three edges of the triangular patch.

IV. PO FORMULATIONS ON TRIANGULAR PATCHES BY THE NSDP METHOD

After finding the NSDPs in Section III, we give the result of PO surface integral formulations in (4) on triangular patches. Firstly, the surface PO integral defined on Δ_1 in Fig. 5(a) can be separated into three line integrals

$$I_{\Delta_1} = I_2^{(a_1,b_1)} + I_2^{(a_2,b_2)} - I_2^{(a_3,b_3)}. \quad (19)$$

Then, on invoking the Cauchy's integral formulation and following the similar mathematical manipulations as those in [19], the above three highly oscillatory line integrals can be rewritten as

$$I_2^{(a_1,b_1)} = I_{2,\mathbf{V}_{1,x}}^{(a_1,b_1)} - I_{2,\mathbf{V}_{2,x}}^{(a_1,b_1)} \quad (20)$$

$$I_2^{(a_2,b_2)} = I_{2,\mathbf{V}_{2,x}}^{(a_2,b_2)} + I_{2,\mathbf{X}_{r,2,x}}^{(a_2,b_2)} - I_{2,\mathbf{V}_{3,x}}^{(a_2,b_2)} + K_2((\mathbf{V}_{3,x}, 0)) - K_2\left(\mathbf{A}^{(2)}\right) \quad (21)$$

$$I_2^{(a_3,b_3)} = I_{2,\mathbf{V}_{1,x}}^{(a_3,b_3)} + I_{2,\mathbf{X}_{r,3,x}}^{(a_3,b_3)} - I_{2,\mathbf{V}_{3,x}}^{(a_3,b_3)} + K_2((\mathbf{V}_{3,x}, 0)) - K_2\left(\mathbf{C}^{(3)}\right). \quad (22)$$

Here, in (20)-(22), $\mathbf{V}_n = (\mathbf{V}_{n,x}, \mathbf{V}_{n,y})$ denotes the vertex points of Δ_1, $n = 1, 2, 3$. The variables $\mathbf{V}_{n,x}, \mathbf{V}_{n,y}$ represent the x- and y- values of the vertex points $\mathbf{V}_n$. $\mathbf{A}^{(2)}$ and $\mathbf{C}^{(3)}$ denote the intersection points between the NSDPs and the Stokes' line [19]. The superscripts "2" and "3" represent the second and third edges of the triangular patch, as shown in Fig. 4. The resonance points $\mathbf{X}_{r,m}$ in Fig. 5(a) are denoted as

$$\mathbf{X}_{r,m} = (\mathbf{X}_{r,m,x}, \mathbf{X}_{r,m,y}) = \left(\frac{a_m b_m}{1-a_m^2}, \frac{b_m}{1-a_m^2}\right) \quad (23)$$

a_m and b_m correspond to the variables from three edges of Δ_1, with the formulations $y_m(x) = a_m x + b_m$, $m = 2, 3$. The above $I_{2,\mathbf{V}_{m,x}}^{(a_n,b_n)}$ and $I_{2,\mathbf{X}_{r,m,x}}^{(a_n,b_n)}$ in (20)-(22) are similar as (30)-(31) given in [19] except the different NSDPs in (17) are adopted. And $K_2(x)$ takes the formulation

$$K_2(x) = \left(\frac{\pi}{2k}\alpha_1 + \frac{\pi}{4ik^2}\alpha_4 - \frac{\pi}{4ik^2}\alpha_5\right)\mathrm{erfc}\left(\sqrt{ikx}\right) + \left(\frac{\sqrt{\pi}}{2ik\sqrt{-ik}}\alpha_2 + \frac{\sqrt{\pi}x}{2ik\sqrt{-ik}}\alpha_4\right)e^{-ikx^2}. \quad (24)$$

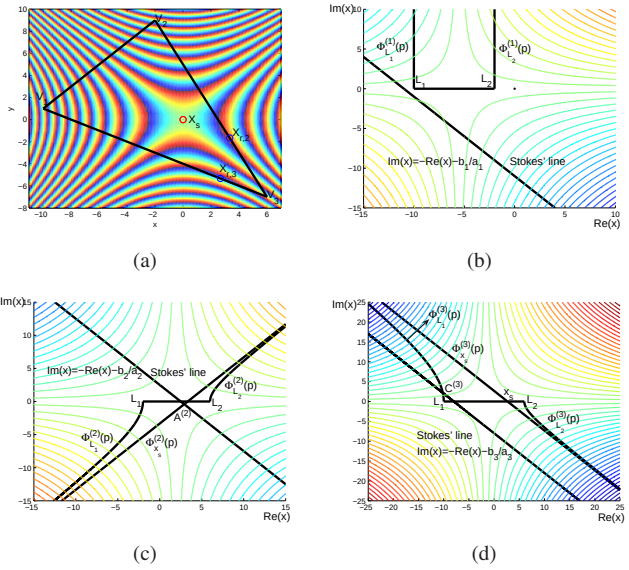

Fig. 5. (a) PO surface integral $I_{\triangle_1}$ defined on the triangular patch, Δ_1. (b) NSDPs diagram for $I_2^{(a_1,b_1)}$ defined on the edge $\mathbf{V}_1\mathbf{V}_2$ of Δ_1. (c) NSDPs diagram for $I_2^{(a_2,b_2)}$ defined on the edge $\mathbf{V}_2\mathbf{V}_3$ of Δ_1. (d) NSDPs diagram for $I_2^{(a_3,b_3)}$ defined on the edge $\mathbf{V}_1\mathbf{V}_3$ of Δ_1.

Remark 2. The PO surface integral can always be reduced to highly oscillatory integrals defined on polygonal edges. In other words, for assembled triangular patches, internal vertex and resonance points contributions are canceled with each other [18].

A. Analysis of critical-point contributions by the NSDP method

When the working frequency is high, the PO based EM fields in (1) can be separated into high frequency critical points contributions [2], [7]. In Fig. 5(a), these critical points consist of the stationary phase point $\mathbf{X}_s$ (SPP), the boundary resonance points $\mathbf{X}_{r,m}$ (RSPs) and the vertex points $\mathbf{V}_n$ (Vexs), $m = 2, 3$, $n = 1, 2, 3$.

Similarly to the discussions in [20], on invoking the NSDP method, the critical points contributions for the PO integral in

(19) take the forms

$$I_{\triangle_1}^{(\text{NSDP, SPP})} = \underbrace{K_2\left(\mathbf{C}^{(3)}\right) - K_2\left(\mathbf{A}^{(2)}\right)}_{\text{contributions from } l_{\text{Stokes}}} \quad (25)$$

$$I_{\triangle_1}^{(\text{NSDP, RSPs})} = \underbrace{I_{2,\mathbf{X}_{r,2,x}}^{(a_2,b_2)} - I_{2,\mathbf{X}_{r,3,x}}^{(a_3,b_3)}}_{\text{contributions from two RSPs}} \quad (26)$$

$$I_{\triangle_1}^{(\text{NSDP, Vexs})} = \underbrace{I_{2,\mathbf{V}_{1,x}}^{(a_1,b_1)} - I_{2,\mathbf{V}_{1,x}}^{(a_3,b_3)} + I_{2,\mathbf{V}_{2,x}}^{(a_2,b_2)} - I_{2,\mathbf{V}_{2,x}}^{(a_1,b_1)}}$$
$$+ \underbrace{I_{2,\mathbf{V}_{3,x}}^{(a_3,b_3)} - I_{2,\mathbf{V}_{3,x}}^{(a_2,b_2)}}_{\text{contributions from three vertex points}}. \quad (27)$$

Here, $I_{\triangle_1}^{(\text{NSDP, SPP})}$, $I_{\triangle_1}^{(\text{NSDP, RSPs})}$ and $I_{\triangle_1}^{(\text{NSDP, Vexs})}$ denote the contributions coming from $\mathbf{X}_s$, $\mathbf{X}_{r,m}$ and $\mathbf{V}_n$, respectively. As a result, comparing (25)–(27) with $I_{\triangle_1}$ in (19), we arrive at

$$I_{\triangle_1} = I_{\triangle_1}^{(\text{NSDP, SPP})} + I_{\triangle_1}^{(\text{NSDP, RSPs})} + I_{\triangle_1}^{(\text{NSDP, Vexs})}. \quad (28)$$

The above critical-point contributions via the HFA method are presented in [9], [14], [20]. Furthermore, by the HFA theory, the asymptotic behaviors of contributions coming from SPP, RSPs and vertices, are of orders $O\left(k^{-1}\right)$, $O\left(k^{-1.5}\right)$ and $O\left(k^{-2}\right)$, respectively. In other words, the specular reflection contribution by the SPP is the dominant term in the PO based EM fields [9], [14]. Furthermore, we shall note the similarity and difference of the uniform asymptotic solutions in [9] and [14]. By performing uniform asymptotic techniques in [9] and [14] for high frequency critical points, non-uniform leading terms have the similar formulations. However, when the observation points lie around shadow boundaries, formulations are different in [9] and [14]. Thus, different accuracies in [9] and [14] will be generated from asymptotic solutions.

V. Numerical Results

We first consider the coalescence of the critical points on the triangular patch with the hyperbolic phase behavior, which are shown in Fig. 6(a). The triangular patches are moving along a line $l(x) = 0.5x$, $x \in [-3, 5]$. In particular, with $x = -2$, the edge $\mathbf{V}_2\mathbf{V}_3$ is governed by the line $y = -2x$. Then, the stationary phase point $\mathbf{X}_s$ and the resonance point $\mathbf{X}_{r,3}$ come together. As is seen from Fig. 6(b), the contributions by the NSDP and brute force methods agree well with each other, even when $\mathbf{X}_s$ and $\mathbf{X}_{r,3}$ come together. To compare the results among the NSDP, the HFA and the BF methods, we consider the case $x = 0$. Then, the SPP lies inside of the triangular patch. The PO integral results are $I_\triangle = 0.0291, 0.0290, 0.0278$ by the NSDP, BF and HFA methods.

We consider the hyperbolic surface in Fig. 2(a). The governing equation of the hyperbolic surface is $f(x, y) = 1 - 0.06\left(-x^2 + xy + y^2\right)$. The resultant PO based EM fields is expressed in (1). $\partial\Omega_{xy}$ is the quadrilateral domain $\overline{\mathbf{V}_1\mathbf{V}_2\mathbf{V}_3\mathbf{V}_4}$ shown in Fig. 2(b), with the vertex points $\mathbf{V}_1 = (-5.6036, 0.7987)$, $\mathbf{V}_2 = (2.3455, 5.7115)$, $\mathbf{V}_3 = (2.9254, -4.1142)$, and $\mathbf{V}_4 = (8.9043, 5.0974)$. The incident wave propagates along $\hat{\mathbf{r}}^{(i)} = \left[0.5, 0.5, -\sqrt{2}/2\right]$ direction, and the observation point is set along the direction $\hat{\mathbf{r}} = \left[\sqrt{2}/4, \sqrt{6}/4, \sqrt{2}/2\right]$.

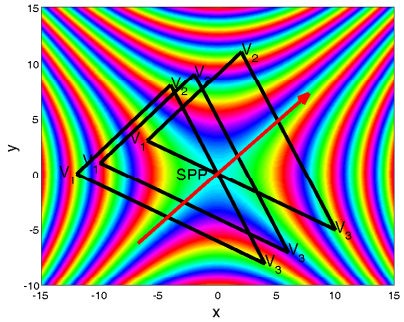

(a)

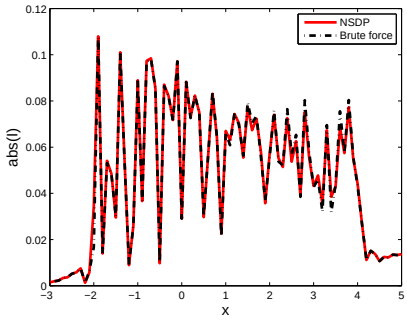

(b)

Fig. 6. (a) PO surface integral $I_\triangle$ defined on the triangular patches, which are moving along the line $l(x) = 0.5x$ denoted by the red color row. (b) Amplitude of the PO surface integrals from the triangular patches that are moving along the line $l(x) = 0.5x$, $x \in [-3, 5]$.

By applying the NSDP method, we could generate the PO based EM fields results. Meanwhile, another way to generate PO based EM fields results is the HFA method [7], [9]. In this paper, we consider the case that the critical points are isolated. Hence, we adopt the non-uniform solutions for the PO based EM fields. Meanwhile, we note that critical points transitional behaviors are neglected in the asymptotic analysis, which leads to low accuracy results generated for the PO based EM fields. If the uniform asymptotic technique with the UTD transition function is adopted, one could estimate high accuracy as the consideration of transitional contributions for critical points. We will consider the uniform-asymptotic technique in the future.

In Fig. 7, we apply the NSDP method to calculate the bistatic RCS values of $\mathbf{E}^{(s)}(\mathbf{r})$, which are in good agreement with the results generated by the BF method. Fig. 8 demonstrates the frequency independent computational effort for the scattered electric field. Finally, Table I gives comparisons of the errors of $\mathbf{E}^{(s)}(\mathbf{r})$ produced by NSDP and HFA methods relative to the BF method. Compared with the HFA method, the advantage on improving the scattered electric field accuracy by the NSDP method is again confirmed in Table I. In summary, on invoking the proposed NSDP method, the PO based EM fields on the quadratic hyperbolic surface could be calculated with frequency independent workload and error controllable accuracy.

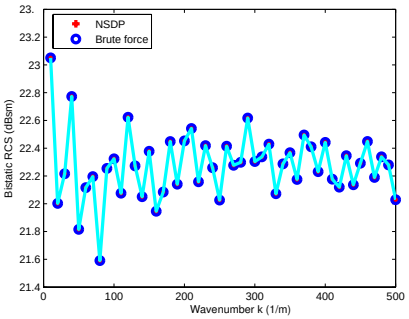

Fig. 7. Comparisons of the RCS (dBsm unit) values of the PO based EM fields on the hyperbolic surface by using the NSDP and BF methods.

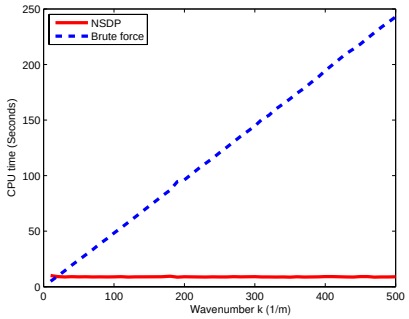

Fig. 8. Comparisons of the CPU time (second unit) for the PO based EM fields by using the NSDP and BF methods.

VI. Conclusion

In this communication, we propose the NSDP method to calculate the PO based EM fields on the quadratic hyperbolic surface. The scattered electric field can be reduced to several highly oscillatory PO surface integrals. By deforming the original PO integration path to the numerical steepest descent path on the complex plane, each PO integrand decays exponentially. Extensive numerical experiments are given to show the efficiency of the NSDP method. In conclusion, the NSDP method for calculating the electric scattered field on the quadratic hyperbolic surface is frequency independent and error controllable.

References

[1] H. M. Macdonald, "The effect produced by an obstacle on a train of electric waves," *Phil. Trans. Royal Soc. London, Series A, Math. Phys. Sci.*, vol. 212, pp. 299–337, 1913.

[2] W. C. Chew, *Waves and Fields in Inhomogeneous Media.* New York: IEEE Press, 1995.

TABLE I
Comparisons of the errors of $\mathbf{E}^{(s)}(\mathbf{r})$ results by using the NSDP and HFA methods relative to the BF method.

k (1/m)	HFA–Error	NSDP–Error	NSDP–CPU	BF–CPU
10	4.613342E–3	5.719708E–9	10.1089	4.9296
50	6.244134E–4	1.450380E–13	8.9077	24.0866
100	1.225014E–4	7.211293E–12	8.8609	48.2979
200	7.728819E–5	4.616638E–8	8.9857	96.1590
300	3.698174E–5	1.144945E–5	8.6581	169.0427
500	1.945051E–5	4.181301E–5	8.9701	242.8624

[3] J. A. Kong, *Electromagnetic Wave Theory.* New York: Wiley-Interscience, 1990.

[4] A. C. Ludwig, "Computation of radiation patterns involving numerical double integration," *IEEE Trans. Antennas Propag.*, vol. 16 , no. 6, pp. 767–769, June 1968.

[5] R. J. Burkholder and T. Lee, "Adaptive sampling for fast physical optics numerical integration," *IEEE Trans. Antennas Propag.*, vol. 53, no. 5, pp. 1843–1845, May 2005.

[6] A. Iserles and D. Levin, *Asymptotic expansion and quadrature of composite highly oscillatory integrals*, Math. Comp., 80 (2011), pp. 279–296.

[7] R. G. Kouyoumjian, "Asymptotic high-frequency methods," *Proceedings of the IEEE*, vol. 53, pp. 864–876, 1965.

[8] O. M. Conde, J. Pérez, and M. F. Cátedra, "Stationary phase method application for the analysis of radiation of complex 3-D conducting structures," *IEEE Trans. Antennas Propag.*, vol. 49, no. 5, pp. 724–731, May 2001.

[9] G. Carluccio, M. Albani, and P. H. Pathak, "Uniform asymptotic evaluation of surface integrals with polygonal integration domains in terms of UTD transition functions," *IEEE Trans. Antennas Propag.*, vol. 58, no. 4, pp. 1155–1163, Apr. 2010.

[10] C. D. Giovampaola, G. Carluccio, F. Puggelli, A. Toccafondi, and M. Albani, "Efficient algorithm for the evaluation of the physical optics scattering by NURBS surfaces with relatively general boundary condition," *IEEE Trans. Antennas Propag.*, vol. 61, no. 8, pp. 4194–4203, Aug. 2013.

[11] G. Carluccio, F. Puggelli, and M. Albani, "Algorithm for the Computation of the Generalized Fresnel Integral," *IEEE Trans. Antennas Propag.*, vol. 59, no. 10, pp. 3943–3947, Oct. 2011.

[12] F. Puggelli, G. Carluccio, and M. Albani, "An Efficient Algorithm for the Computation of the UTD T Transition Function," *IEEE Trans. Antennas Propag.*, vol. 60, no. 5, pp. 2380–2387, May 2012.

[13] R. Wong, *Asymptotic Approximations of Integrals*. New York: SIAM, 2001.

[14] V. A. Borovikov, *Uniform Stationary Phase Method*. London: Institution of Electrical Engineers, 1994.

[15] M. Abramowitz and I. A. Stegun, *Handbook of Mathematical Functions.* Norwood: MA, Dover, 1972.

[16] A. Asheim and D. Huybrechs, *Asymptotic analysis of numerical steepest descent with path approximations*, Found. Comput. Math., 10 (2010), pp. 647–671.

[17] F. V. Bondia, M. F. Bataller, and A. V. Nogueira, "A new fast physical optics for smooth surfaces by means of a numerical theory of diffraction," *IEEE Trans. Antennas Propag.*, vol. 58, no. 3, pp. 773–789, Mar. 2010.

[18] Y. M. Wu, L. J. Jiang, and W. C. Chew, "An efficient method for computing highly oscillatory physical optics integral," *Progr. Electromagn. Res. PIER*, vol. 127, pp. 211–257, 2012.

[19] Y. M. Wu, L. J. Jiang, W. E. I. Sha, and W. C. Chew, "The numerical steepest descent path method for calculating physical optics integrals on smooth conducting surfaces," *IEEE Trans. Antennas Propag.*, vol. 61, no. 8, pp. 4183-4193, Aug. 2013.

[20] Y. M. Wu, L. J. Jiang, and W. C. Chew, "Computing highly oscillatory physical optics integral on the polygonal domain by an efficient numerical steepest descent path method," *J. Comput. Phys.*, vol. 236, pp. 408–425, Mar. 2013.

[21] H. T. Chou and J. T. Johnson, "A novel acceleration algorithm for the computation of scattering from rough surfaces with the forwards-backward method," *Radio Science*, vol. 33, no. 5, pp. 1277–1287, Sep. 1998.

[22] L. Rodriguez, K. Yukimasa, T. Shijo, and M. Ando, "Inner stationary phase point contribution of physical optic in terms of the modified edge representation line integrals (curved surfaces)," *Radio Science*, vol. 42, no. 5, RS6S24, pp. 1-8, 2007.

[23] R. G. Kouyoumjian and P. H. Pathak, "A uniform geometrical theory of diffraction for an edge in a perfectly conducting surface," *Proc. IEEE*, vol. 62, no. 11, pp. 1448–1461, Nov. 1974.

[24] S. C. Tuan and H. T. Chou, "Analytic solution of transient scattering fields from a hyperbolic surface illuminated by a plane wave," *2015 Asia-Pacific Symposium on Electromagnetic Compatibility (APEMC)*, pp. 306–308, 2015.